Tribol Lett (2014) 53:119–126
DOI 10.1007/s11249-013-0250-7

ORIGINAL PAPER

Wear, Plasticity, and Rehybridization in Tetrahedral Amorphous Carbon

Tim Kunze · Matthias Posselt · Sibylle Gemming · Gotthard Seifert · Andrew R. Konicek · Robert W. Carpick · Lars Pastewka · Michael Moseler

Received: 9 July 2013 / Accepted: 14 October 2013 / Published online: 31 October 2013

Abstract Wear in self-mated tetrahedral amorphous carbon (ta-C) films is studied by molecular dynamics and near-edge X-ray absorption fine structure spectroscopy. Both theory and experiment demonstrate the formation of a soft amorphous carbon (a-C) layer with increased sp^2 content, which grows faster than an a-C tribolayer found on self-mated diamond sliding under similar conditions. The faster $sp^3 \rightarrow sp^2$ transition in ta-C is explained by easy breaking of prestressed bonds in a finite, nanoscale ta-C region, whereas diamond amorphization occurs at an atomically sharp interface. A detailed analysis of the underlying rehybridization mechanism reveals that the $sp^3 \rightarrow sp^2$ transition is triggered by plasticity in the adjacent a-C. Rehybridization therefore occurs in a region that has not yet experienced plastic yield. The resulting soft a-C tribolayer is interpreted as a precursor to the experimentally observed wear.

T. Kunze (✉) · G. Seifert
Theoretical Chemistry, University of Technology Dresden, 01662 Dresden, Germany
e-mail: t.kunze@hzdr.de

M. Posselt · S. Gemming
Helmholtz-Zentrum Dresden-Rossendorf, P.O. Box 51 01 19, 01314 Dresden, Germany

A. R. Konicek · R. W. Carpick
Department of Mechanical Engineering and Applied Mechanics, University of Pennsylvania, Philadelphia, PA 19104, USA

L. Pastewka · M. Moseler
Fraunhofer-Institut für Werkstoffmechanik IWM, Wöhlerstrasse 11, 79108 Freiburg, Germany
e-mail: michael.moseler@iwm.fraunhofer.de

Keywords Wear · Plasticity · Rehybridization · ta-C · Tribology

1 Introduction

Tetrahedral amorphous carbon (ta-C) coatings have attracted substantial scientific and technological attention in recent years because they show low friction in humid environments and have superior resistance to abrasive as well as adhesive wear [1, 2]. These tribological properties make ta-C an outstanding candidate for protective coatings that reduce wear and friction in micro- and macromachines [3]. Nevertheless, ta-C coatings abrade slowly, even under lubricated conditions, and the detailed wear mechanism is typically hidden by the complex passivation processes at the sliding interface. Experimentally, wear is accompanied by the formation of a surface layer with an increased amount of sp^2-hybridized amorphous carbon compared to the bulk of the film [4–6]. This suggests a partial loss of surface passivation and subsequent covalent interaction across the interface during sliding [7]. Interactions of contacting asperities must then involve plastic deformation of the amorphous carbon (see Ref. [8] for a review on plasticity in glassy materials) and eventually fracture.

In general, the coatings low friction can be attributed to a rapid repassivation (after asperity interactions) of dangling surface bonds by species such as dissociated ambient H_2O molecules [9]. Here, we propose that their wear resistance can be linked to an entirely different process, namely shear localization during deformation of the diamond-like sp^3 network. It is well known that bulk amorphous metals fail through such shear bands [10]. Our molecular dynamics simulations of ta-C/ta-C tribocouples indicate that ta-C also localizes shear, in this case at the

sliding interface. Shear is accompanied by a gradual transformation or rehybridization into a softer sp^2-rich phase. This is supported by near-edge X-ray absorption fine structure (NEXAFS) spectroscopy analysis of worn ta-C that shows a comparable $sp^3 \rightarrow sp^2$ rehybridization. We contrast these results to the behavior of diamond tribocouples. In all cases, theory and experiment show that the observed formation rate of amorphous carbon (a-C; having significantly more sp^2 than ta-C) in the ta-C/a-C/ta-C system exceeds the amorphization rate in diamond/diamond tribocouples under similar conditions [11]. We propose that, ultimately, the weak sp^2 phase succumbs to wear, but also prevents fatal events such as microfracture of asperities and formation of wear debris. The rehybridization rate therefore limits the overall wear rate.

Rehybridization shows that the previously introduced shear banding is accompanied by a change in local order of the material [12, 13]. Mesoscopic models of plasticity rely on some order parameter (or collective variable) that characterizes the degree of local order. Examples are the effective temperature in shear transformation zone theory, or the liquid like material concentration in amorphous silicon [14–16]. The fraction of sp^3-coordinated carbon atoms or sp^3 hybridization is such an order parameter that has the added advantage of being experimentally accessible. A typical evolution equation then couples the order parameter field to the locally integrated amount of local plastic strain [17]. In contrast, our simulations reveal a nonlocal coupling between strain rate and rehybridization. This rehybridization precedes plastic events, and the material is weakened before it yields. This is possible because a large fraction of bonds in ta-C are already severely prestressed and require only minute perturbation to break. The diamond/diamond tribocouple shows similar shear localization, but the diamond to a-C transformation is confined to a region of low but finite shear rate [11].

2 Methods

2.1 Molecular Dynamics Simulation

We create two independent ta-C films by a simulated liquid carbon quench from two opposing diamond surfaces, producing a stack of two 2.9 nm × 3.0 nm × 5.5 nm ta-C films with roughly 70 % sp^3 concentration. The ta-C film structure agrees well with reported data on simulated growth of ta-C thin films [18, 19]. Periodic boundary conditions are applied in lateral directions. No additional surface chemical termination is added, as we assume that surface species will be mechanically peeled off during asperity collisions, or will eventually dissociate due to sliding-induced heat and subsequent destabilization [20, 21]. Both processes lead to welding (covalent bond formation) across the interface. Hence, we cut the two films to expose bare ta-C surfaces and pair them to form a sliding system with an incommensurate, poorly-bonded plane where sliding initiates. This sliding setup is similar to previous simulations of self-mated ta-C surfaces [7]. The top and bottom section of the sliding system is subdivided into three layers as described in Refs. [22, 23]. The atomic positions of the outermost 0.4 nm layer is fixed, and a $T = 300$ K Langevin thermostat is applied to an adjacent 0.6-nm-wide layer. The motion of the remaining atoms between the two thermostated layers of each film is calculated from Newton's equations. We employ the second-generation reactive empirical bond-order potential (REBO2) [24] with an improved nearest-neighbor cutoff scheme [19, 25]. The modified cutoff scheme is mandatory for a reasonable description of bond-breaking and formation processes during friction. A load of 10 GPa is then applied to the fixed atoms of the upper ta-C film. The construction of our barostat compensates for the finite size of the simulated system [22]. A sliding velocity of $v_S = 20$ m s^{-1} is instantly applied to the upper fixed layer. By construction, the initial ta-C/ta-C tribocouple consist of two 70 % sp^3 ta-C films separated by a 0.4-nm layer of a-C. An equivalent simulation setup, as described for the ta-C case, was chosen for the diamond tribocouples.

2.2 Experiments

The details of the sample preparation, tribological tests, and NEXAFS characterization are presented in Ref. [4]. In brief, Si flats and 3-mm-diameter Si_3N_4 spheres were simultaneously coated with either ta-C or ultrananocrystalline diamond (UNCD). The ta-C films were deposited using a pulsed laser deposition technique with a thickness of ~1 μm and subjected to a standard post-growth anneal to relieve residual stress. UNCD was deposited by a microwave plasma chemical vapor deposition technique with a thickness of 1–2 μm. The UNCD films had a typical as-grown surface roughness of ~11 nm r.m.s. over a 1 × 1 μm^2 area, 2–5 nm grains, and exhibit 95–98 % sp^3 bonding overall. The ta-C films have an as-grown surface roughness of ~0.1 nm r.m.s. over a 1 × 1 μm^2 area and are comprised of an amorphous network of carbon that has been measured independently to be ~80 %sp^3-bonded, with the remaining ~20 % being sp^2-bonded.

After deposition, these films were subjected to self-mated reciprocating tribometry tests using a tribometer housed inside an environmental chamber. Normal and lateral forces were measured with a calibrated dual flexure cantilever. In all cases, 5,000 sliding cycles were performed to ensure steady-state friction behavior. The reciprocation length was set to 600 μm for every track,

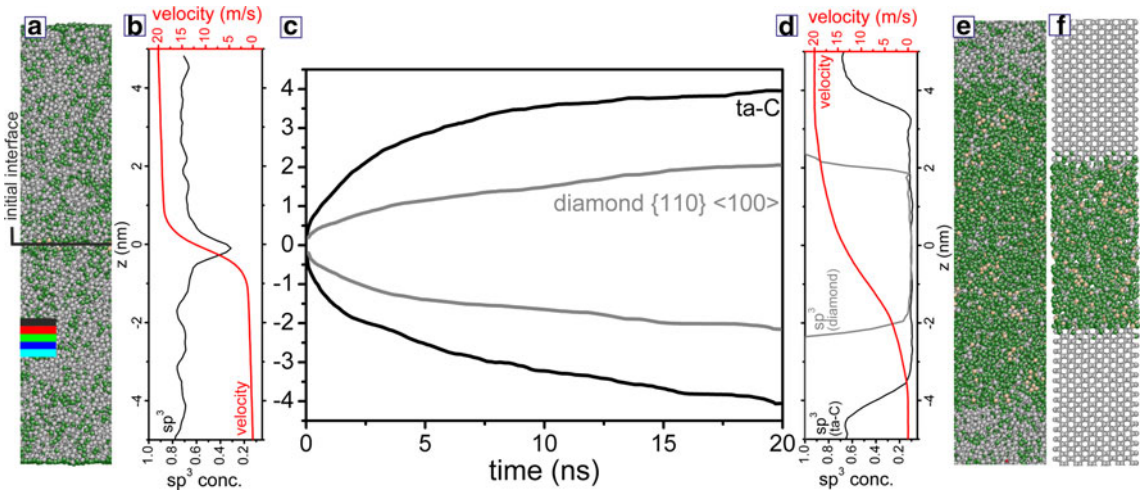

Fig. 1 (Color online) **a** side-view snapshot of the ta-C/ta-C tribosystem after 0.1 ns of sliding. Atoms are color-coded according to their atomic coordination: *white* → 4-fold (sp^3), *green* → 3-fold (sp^2), *yellow* → 2-fold (sp^1). The *colored bars* define layers that were used for further analyses in Fig. 3. **b** sp^3 concentration (*black curve*) and velocity profile (*red curve*) across the ta-C/ta-C tribocouple. **c** Evolution of the upper and lower boundary of the a-C tribofilm formed between two ta-C surfaces (*black curve*) compared to a corresponding film formed between two diamond {110} surfaces rubbed in ⟨100⟩ direction (*gray curve*). **d** sp^3 concentration (*black curve* for ta-C and *gray curve* for diamond) and velocity profile of the ta-C system (*red curve*) after 20 ns of sliding. **e** and **f** is a side-view snapshot of the ta-C/ta-C and diamond/diamond tribosystems after 20 ns sliding

with a sliding speed of 2.5 mm s^{-1}. Humidity was introduced by controlling the flow of dry argon through a beaker containing deionized water and measured with a DewPro MMY 2650 hygrometer, which is accurate within 0.1 %, with a lower detection limit of 0.1 %. Experiments were conducted at different loads and humidity values. The results presented here were for an applied load of 0.1 N for UNCD, corresponding to an initial mean Hertzian contact pressure of 300 MPa, and 0.05 N for ta-C, corresponding to an initial mean Hertzian contact pressure of 240 MPa. The relative humidity used was 1.0 %.

The wear tracks were analyzed ex-situ using photoelectron emission microscopy (PEEM) (beamline 7.3.1.1 at the advanced light source), which is a surface-sensitive technique that characterizes the top ~4 nm of the sample with ~100-nm lateral resolution. The chemical information is obtained from the NEXAFS spectra acquired in conjunction with the spatial information of PEEM. The spectra acquired predominantly came from the center of each track.

3 Tribosimulation of ta-C

Figure 1a shows a snapshot of the ta-C/ta-C tribosystem after 0.1 ns of sliding. The initial a-C layer is clearly associated with a drop in the sp^3 concentration profile in Fig. 1b and accommodates all sliding-induced shear (see velocity profile in Fig. 1b). With continuous sliding, the region near the contact interface undergoes a phase transition from sp^3 to sp^2 hybridized carbon, which leads to the formation of additional a-C tribomaterial between the ta-C regions. This is consistent with earlier simulation on the initial (<200 ps) stage of sliding at around 90 m s^{-1} [7]. Note that Ref. [7] reports the formation of a significant smaller tribofilm than in the present work at comparable load and sliding distance, although the mechanical stability of our investigated film is significantly higher. This difference could be related to slight differences in the simulation methodology [19, 26]. The width of our a-C interlayer grows with increasing sliding distance (black curve in Fig. 1c) and exhibits a square-root-like dependence in time, similar to the a-C that forms between sliding diamond surfaces [11]. For comparison, the gray curve in Fig. 1c shows the pairing of the softest diamond tribocouple that exhibits a significantly slower growth of the a-C interlayer.

An explanation for this marked difference in growth rate could be an elevated temperature at the ta-C/a-C interface since the thermal conductivity of ta-C is lower than that of single crystal diamond. Indeed, we find T = 490 K at the ta-C/a-C interface while diamond shows T = 350 K in the vicinity of the formed a-C [11]. On the other hand, the temperature for ta-C is well below its melting point, which is estimated at 4,000 K [27]. Therefore, melting can be ruled out as the driving force for the $sp^3 \rightarrow sp^2$ transition and a mechanically driven rehybridization process is proposed instead (as it has already been discussed in Ref. [11] for diamond).

For both ta-C/ta-C and diamond/diamond, after 20 ns of sliding a rather homogeneous distribution of 70–80 % sp^2 carbon with equal sp^1 and sp^3 fractions can be detected

within the a-C tribolayers. This is illustrated in the sp^3 concentration profiles in Fig. 1d and the atomic structure of the ta-C system in Fig. 1e. Furthermore, the $sp^3 \rightarrow sp^2$ transition region spreads over a 1-nm-wide layer, in contrast to the sharp diamond/a-C interface in the diamond simulations. The corresponding ta-C (black) and diamond (gray) sp3 profiles in Fig. 1d clearly show the extent of this transition region where the distinct diamond/a-C interface also clearly appears in the atomic structure in Fig. 1f. Interestingly, the ta-C/a-C $sp^3 \rightarrow sp^2$ transition region is not taking part in the shear process. All tribo-induced plasticity is restricted to the soft, high-sp^2 region as seen by comparing the velocity profile (red) to the hybridization profile (black) in Fig. 1d.

4 Experimental Evidence of a-C Tribofilm

Wear experiments on ta-C and diamond support our theoretical results. We analyzed the NEXAFS spectra from Ref. [4] to estimate the amount of a-C that is formed in ta-C/ta-C and diamond/diamond pairings. Figure 2 shows the difference between spectra taken from the heavily worn and unworn ta-C and UNCD surfaces on the flat, respectively. The difference signal for the ta-C case is presented relative to the UNCD difference, where the latters C 1s $\rightarrow \pi^*$ peak height had been normalized to unity. In both cases, the magnitude of the C 1s $\rightarrow \pi^*$ peak at 285 eV (a feature unique to sp^2-bonded C) is significantly increased. Thus, a noticeable conversion from sp^3-to sp^2-bonded carbon occurs in ta-C as well as in diamond, which corroborates our simulations. Moreover, the increase in the C 1s $\rightarrow \pi^*$ peak was more than two times higher for ta-C than for UNCD, which demonstrates a significantly higher sp^3-to sp^2- conversion rate in ta-C. This was found consistently for all loads and relative humidities (RHs) investigated in Ref. [4], respectively, as long as the silicon substrate stayed intact (plastic deformation of the Si substrate was observed in some cases when loads and friction forces were high, rendering it difficult to compare with other cases as this meant that contact areas and stresses were significantly altered). Note that a quantitative comparison with our atomistic simulations is impossible, since topographical differences, gas environment, surface passivation, and film/substrate effects are neglected in our model. Nevertheless, it is striking that the amount of sp^3-to sp^2 conversion is always more pronounced for ta-C/ta-C than for UNCD/UNCD pairings irrespective of the load or RH. These findings, and especially the similar track wear rates at different RH for low loads, suggest only a secondary influence of the test conditions on the rehybridization mechanism.

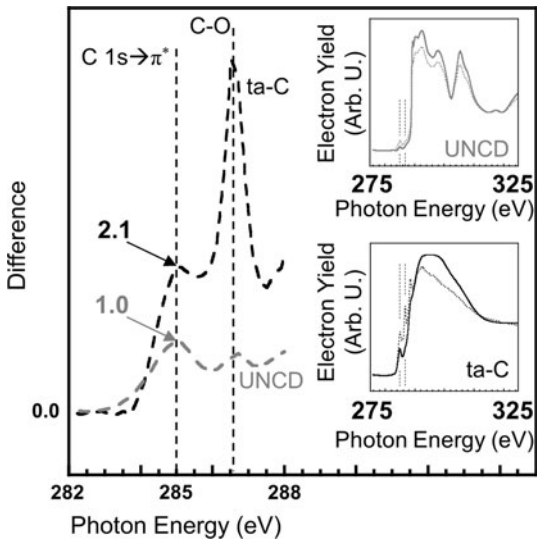

Fig. 2 Difference in NEXAFS total electron yield spectra between worn and unworn regions of carbon-based films. *Gray curve* difference between a spectrum taken from a heavily modified region of the UNCD wear track and a spectrum from unworn UNCD, where the C 1s $\rightarrow \pi^*$ peak height was normalized to unity. *Black curve* difference between a spectrum taken from a heavily modified region of the ta-C wear track and a spectrum from unworn ta-C with respect to the UNCD difference. The *upper inset* shows the worn (*gray*) UNCD spectrum and the unworn (*black*) UNCD spectrum. The *lower inset* shows the worn (*gray*) ta-C spectrum and the unworn (*black*) ta-C spectrum. Note, that even in the unworn spectra a small amount of sp^2 is present. This can be explained by grain boundaries [28] or an initial sp^2-rich overlayer [29, 30] in diamond or ta-C, respectively. However, a preexisting sp^2 contribution is eliminated in the difference spectra by subtraction. The applied loads were 0.1 N for UNCD, and 0.05 N for ta-C, and measurements were obtained at 1.0 % RH

5 Rehybridization Mechanism

To further study the mechanism that underlies the ta-C/a-C phase transformation, we analyze the evolution of the average sp^3 concentration in a stack of five layers of thickness $\Delta z = 0.2$ nm within the lower ta-C film. Each of these layers, indicated by the colored bars in Fig. 1a, is located between $z = -1.9$ nm and $z = -2.9$ nm below the initial sliding plane. In the five layers, the initial sp^3 concentration is approximately 70 % and, after 20 ns of sliding, this concentration decreases to approximately 10 % (Fig. 3a). The onset of this phase transformation depends on the height of the layers within the lower ta-C film. Horizontal bars in Fig. 3b mark the time interval in which each layer's sp^3 concentration drops from 60 to 20 %, and show clearly that the more distant layers transform later.

Next, we consider the evolution of local shear strain $\gamma(z, t)$ in a layer at height z which is determined from the shear rate $\frac{\partial v(z,t)}{\partial z}$ by $\gamma(z,t) = \int_0^t \mathrm{d}t' \frac{\partial v(z,t')}{\partial z}$. The shear rate within a layer is calculated as a finite difference of the

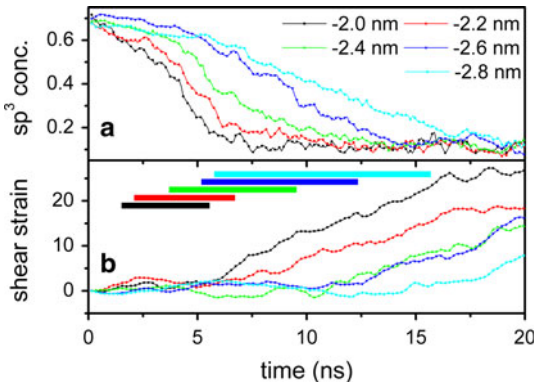

Fig. 3 (Color online) Evolution of sp^3 concentration (**a**) and shear strain (**b**) in the stack of 5 layers as described in the text. The *color code* distinguishes the height of the layers (see also *bars* in Fig. 1a). The *colored bars* in **b** denote the main rehybridization region (transition region between 60 and 20 % sp^3 concentration) of the respective layers

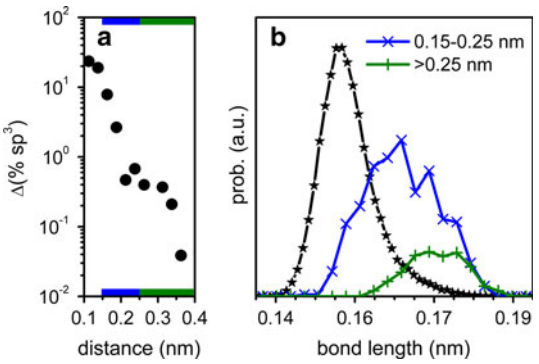

Fig. 4 (Color online) **a** Average change of the sp^3 hybridization depending on the distance from the L/U interface after perturbing the system (according to the auxiliary calculations as described in the text). **b** Distribution of bond length of all bonds with at least one sp^3 hybridized atom. The *black curve* corresponds to all bonds of the unperturbed case. The *blue* and *green curves* depict the subset of the unperturbed distribution that will break within the distance bars highlighted in **a**

velocities $v(z \pm \Delta z/4, t)$ of two sub-layers of height $\Delta z/2 = 0.1$ nm. Figure 3b depicts the evolution of the local strain $\gamma(z, t)$ for the five individual layers. Each layer starts with fluctuations around zero strain followed by a clear transition to a linear increase in strain. Remarkably, this onset of plastic deformation takes place after the layer has transformed to a-C. Note that the end of the colored bars that show the transformation region in Fig. 3b coincides with the onset of plastic strain. Thus, any mechanism that connects the $sp^3 \rightarrow sp^2$ transformation to local plasticity can be ruled out.

On the other hand, it becomes evident from Fig. 3a and b that the ta-C/a-C phase change takes place close to the strained part of the tribosystem. The "black" layer in Fig. 3b starts to yield at roughly 5 ns and, at the same time, the sp^3 concentration of the 0.6 nm deeper lying "blue" layer begins to drop. This suggests that rehybridization must be driven by fluctuations in stress that propagate from the continuously sheared a-C into the stationary ta-C bulk. To test this hypothesis, we investigate the influence of structural rearrangements at the ta-C/a-C interface on deeper lying ta-C layers with an auxiliary simulation. A 5.8-nm-thick ta-C film with 70 % sp^3 concentration and lateral dimensions 2.6 nm × 2.6 nm is split equally into an upper (U) and lower (L) part. The U part is then rigidly shifted by a distance Δx in lateral direction. In this way, the force network at the L/U interface is drastically changed, mimicking the strong plastic events in the a-C of our previous tribosimulation. Finally, the whole system is relaxed [31], and the induced rehybridization is analyzed. Figure 4a depicts the change of the sp^3 content in the vicinity of the L/U interface, which is situated at a distance of 0 nm. These data are obtained as an average over 10 different Δx in 20 independent L/U samples. Besides the expected strong drop of sp^3 near the L/U interface (<0.25 nm away from the perturbation; highlighted by the blue bars), we also observe rehybridization events that are almost 0.4 nm away from the L/U interface (as highlighted by the green bars). This finding clearly indicates that the continuous change of the force network at the ta-C/a-C interface affects the structural integrity of the deeper layers in ta-C and promotes rehybridization.

The resistivity to these force fluctuations can be determined by investigating the bond length distribution in the ta-C film since any event that promotes an sp^3 carbon atom into an sp^2 state requires the breaking of a bond. The black curve in Fig. 4b displays the distribution of bond lengths between all atom pairs with at least one sp^3 hybridized atom (i.e., sp^2–sp^3 and sp^3–sp^3 bonds) *prior* to the rigid shift of U. The same distribution function can be recorded for the subset of these bonds that will be broken *after* the rigid U shift. Figure 4b shows these distributions for bonds that were closer (blue) and further away (green) from the L/U interface. It is apparent that the broken sp^2–sp^3 and sp^3–sp^3 bonds were already elongated and thus weakened *before* the rigid U shift. This suggests that sp^2–sp^3 and sp^3–sp^3 bonds with tensile prestress will break first when exposed to force fluctuations from the changed L/U interface. All sp^2–sp^2 bonds stayed intact during this procedure.

6 Discussion and Conclusions

Both our atomistic simulations and our NEXAFS analysis of ta-C/ta-C and diamond/diamond tribo couples reveal the formation of an amorphous sp^2 (a-C) interlayer. A first guess for the mechanism behind the $sp^3 \rightarrow sp^2$ rehybridization at

the ta-C/a-C and diamond/a-C interface would be graphitization induced by a frictional temperature rise [20] suggesting that the different rehybridization rates result from the different thermal conductivities of the two materials. Although this wear scenario cannot be excluded for extreme tribological loading, the experiments and simulations presented here hint toward another mechanism. We have estimated the temperature rise in the experiment using the approach described in Ref. [20] and find the rise to be below three degrees for both ta-C and UNCD. Note that ta-C and UNCD have comparable thermal conductivities due to the presence of grain boundaries in the latter [32, 33]. The situation is similar in our simulations. The interface temperature in both systems stays well below the corresponding materials' melting temperatures [11, 25, 27]. This shows that heat-induced structural transformations play a secondary role, and consequently, rehybridization is dominated by a tribomechanical rather than a tribothermal process.

Our simulation results show that this tribomechanical process progresses through plastic events that transform the surrounding material to a weaker state even in the presence of highly compressive external stresses. Responsible for this weakening is shear-induced force-fluctuation that is carried by strong bonds in the amorphous network and break its weak bonds. The non-local character of this process is surprising because it is in distinct contrast to current models for plasticity in amorphous materials, where a local strain-plasticity relation is typically observed. While ta-C could be a special case, it is possible that other materials exhibit a similar non-local behavior, particularly ones with directional bonds. The study of this particular phenomenon requires gradients in the order parameter field. Here, those were initially generated through the pairing of two separate ta-C surfaces, while most computational studies of plasticity start from a homogeneous initial configuration in which it is difficult to disentangle non-local effects.

Within this picture, it is easy to understand why the a-C formation rate is smaller in diamond than in ta-C. Since the a-C tribofilms formed in the ta-C/ta-C and diamond/diamond simulations are identical in terms of their hybridization mixture (Fig. 1d), the force fluctuations that are injected into ta-C and diamond by sliding are of the same order of magnitude. However, bulk diamond lacks the structural inhomogeneities that are characteristic for glassy materials. Its bulk bonds can only be prestressed by an external homogeneous shear stress τ (note that for $\tau = 10$ GPa, the related bond length elongation is <0.01 nm). Thus, only bonds at the diamond/a-C interface are weak enough to break, which leads to an atomically sharp diamond/a-C interface and a correspondingly small amorphization rate. Conversely, a significant fraction of the bulk ta-C bonds have tensile prestress (many of them are elongated by more than 0.015 nm) and therefore are easier to break, consequently leading to a higher a-C formation rate, and a $sp^3 \rightarrow sp^2$ transition region of finite size.

Moreover, our simulation results suggest that the underlying nanostructure of the ta-C film determines its detailed wear behavior during tribological loading. The ta-C films prepared for our simulation exhibit a homogeneous lateral distribution of sp^3 states across the film, consequently leading to a smooth rehybridization across the interface. However, an inhomogeneous sp^3 network could lead to a spatially more localized rehybridization and possibly to fracture events and an enhanced formation of wear debris.

Ultimately, the gradual $sp^3 \rightarrow sp^2$ rehybridization observed for ta-C films dissipates shear energy and prevents catastrophic failure through brittle fracture such as that observed on the hardest (111) surface of diamond [11, 34]. Hence, while shear localization is responsible for the failure of bulk glasses, here it is the source of the toughness under tribological loading [10]. In our simulations, the weak character of the a-C tribointerface eventually allows easy failure upon separation of contacting asperities. The resulting exposed surface is a soft a-C layer on a hard ta-C substrate that would be eventually removed through abrasive or chemical processes, which finally lead to the wear observed macroscopically during experiments [35–37].

Figure 5 displays a summary of the anticipated wear mechanisms acting between two ta-C surfaces under environmental conditions. As-grown ta-C films are usually extremely smooth [38], covered with a 1–2-nm-thick layer of a-C [39], and passivated with H and OH groups after contact with water or lubricants [30] (Fig. 5a). During sliding, asperities on the two opposing tribo partners approach each other. In most asperity collisions, sliding-induced strain is localized between the passivation layers and the weak dispersion forces between the two asperities lead to small friction coefficients [30]. However, sometimes passivation is not sufficient, for instance when asperities have too much vertical overlap leading to the peeling-off of functional groups accompanied by cold welding of the collision partners (Fig. 5b). In this case, the rehybridization mechanism described in this article is activated and an a-C layer is formed (green zone in Fig. 5b). Further sliding leads to shear localization in the a-C until finally the two asperities separate presumably after necking [40] (see Fig. 5c) or even debris formation. After separation, highly reactive a-C surface remains with a high density of dangling bonds and linear sp^1 carbon chains [35, 36] ready for passivation reactions with lubricants and environmental gases [30]. The products of some of these

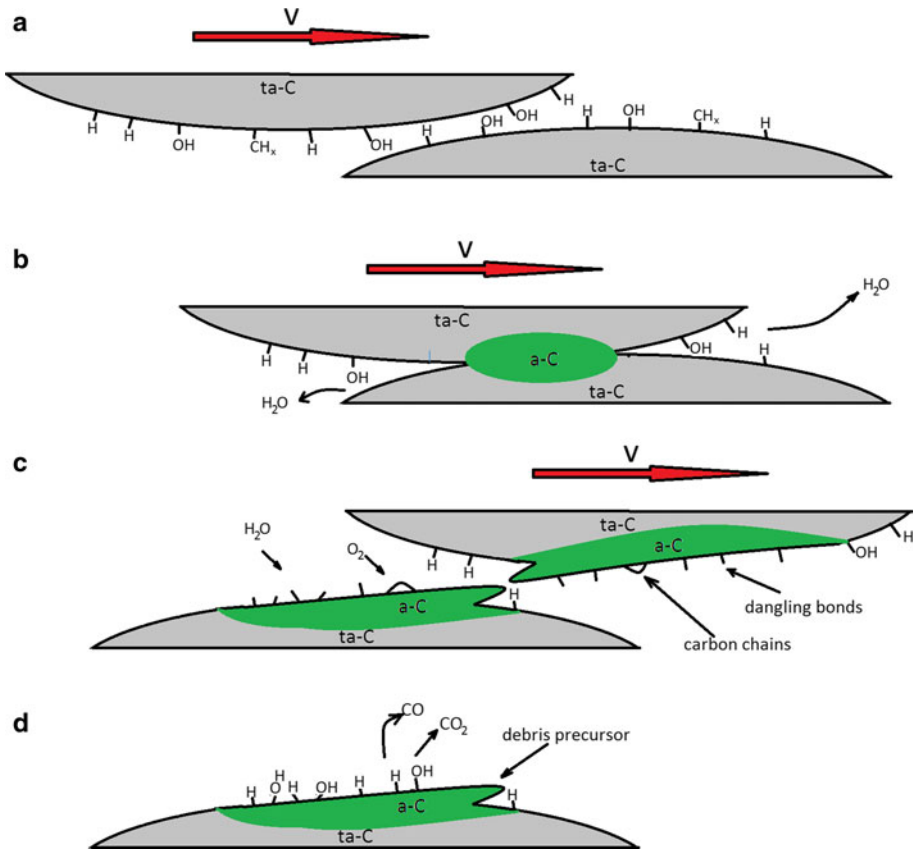

Fig. 5 (Color online) Scenario for wear in tetrahedral amorphous carbon. **a** The collision of two ta-C asperities of a virginal ta-C/ta-C tribo contact. **b** Removal of the passivating species, cold welding of the ta-Cs, and formation of an a-C. **c** Separation of the two asperities is accompanied by formation of dangling bonds, linear carbon chains, and bridge formation. **d** Repassivation after the reaction of the surface radical sites with ambient gases and lubricants

reactions may be gaseous species such as CO and CO_2 (Fig. 5d) resulting in chemical wear of the ta-C [35, 36]. This picture might even hold for hydrogenated amorphous carbon (a-C:H). Recent a-C:H triboexperiments directly revealed a similar sp^2-rich layer after sliding. The authors of this study suggested that sliding produces chemically activated atoms which further react with environmental species [41, 42].

Obviously, rehybridization and passivation can be regarded as competing processes leading to a complex interrelation between friction and wear. Future work is necessary to clarify the potential role of passivating species such as hydrogen and oxygen on the rehybridization mechanism. Nevertheless, the work presented in this article supplies strong support that the interplay of mechano-driven rehybridization (whenever passivation fails) and the subsequent repassivation by environmental species underly the outstanding tribo-performance of ta-C.

Acknowledgements We thank M.L. Falk, P. Gumbsch, M.O. Robbins, and K.M. Salerno for useful discussion. T.K. and G.S. acknowledge funding by the European Center for Emerging Materials and Processes (ECEMP), financed by the European Union and the Free State of Saxony (Project No. 13857 / 2379). R.W.C. and A.R.K. acknowledge support from the Air Force Office of Scientific Research under Contract No. FA2386-11-1-4105 AOARD and from the UPenn MRSEC Program of the National Science Foundation under award No. DMR11-20901. We acknowledge W.G. Sawyer for tribological measurements and useful discussions, A.V. Sumant for providing UNCD films, and T.A. Friedmann for providing ta-C films. L.P. acknowledges funding from the European Commission (Marie-Curie IOF 272619). Computations were carried out at the Jlich Supercomputing Center.

References

1. Robertson, J.: Diamond-like amorphous carbon. Mater. Sci. Eng. R. **37**, 129–281 (2002)
2. Erdemir, A., Donnet, C.: Tribology of diamond-like carbon films. J. Phys. D Appl. Phys. **39**, R311–R327 (2006)
3. Cho, S., Chasiotis, I., Friedmann, T.A., Sullivan, J.P.: Young's modulus, Poisson's ratio and failure properties of tetrahedral amorphous diamond-like carbon for MEMS devices. J. Micromech. Microeng. **15**, 728–735 (2005)
4. Konicek, A.R., Grierson, D.S., Sumant, A.V., Friedmann, T.A., Sullivan, J.P., Gilbert, P.U. P.A., Sawyer, W.G., Carpick, R.W.: Influence of surface passivation on the friction and wear behavior of ultrananocrystalline diamond and tetrahedral amorphous carbon thin films. Phys. Rev. B **85**, 155448 (2012)

5. Konicek, A.R., Grierson, D.S., Gilbert, P.U.P.A., Sawyer, W.G., Sumant, A.V., Carpick, R.W.: Origin of ultralow friction and wear in ultrananocrystalline diamond. Phys. Rev. Lett. **100**, 235502 (2008)
6. Joly-Pottuz, L., Matta, C., de Barros Bouchet, M.I., Vacher, B., Martin, J.M., Sagawa, T.: Superlow friction of ta-C lubricated by glycerol. J. Appl. Phys. **102**, 064912 (2007)
7. Schall, J.D., Gao, G., Harrison, J.A.: Effects of adhesion and transfer film formation on the tribology of self-mated DLC contacts. J. Phys. Chem. C **114**, 5321–5330 (2010)
8. Schuh, C.A., Hufnagel, T.C., Ramamurty, U.: Mechanical behavior of amorphous alloys. Acta Mater. **55**, 4067–4109 (2007)
9. Andersson, J., Erck, R.A., Erdemir, A.: Frictional behavior of diamond-like carbon films in vacuum and under varying water vapor pressure. Surf. Coat. Technol. **163**(164), 535–540 (2003)
10. Pampillo, C.A., Chen, H.S.: Comprehensive plastic deformation of a bulk metallic glass. Mater. Sci. Eng. **13**, 181–188 (1974)
11. Pastewka, L., Moser, S., Gumbsch, P., Moseler, M.: Anisotropic mechanical amorphization drives wear in diamond. Nat. Mater. **10**, 34–38 (2011)
12. Shi, Y., Falk, M.L.: Strain localization and percolation of stable structure in amorphous solids. Phys. Rev. Lett. **95**, 095502 (2005)
13. Widom, M., Strandburg, K.J., Swendsen, R.H.: Quasicrystal equilibrium state. Phys. Rev. Lett. **58**, 706–709 (1987)
14. Falk, M.L., Langer, J.S.: Deformation and failure of amorphous materials. Annu. Rev. Condens. Matter Phys. **2**, 353–373 (2011)
15. Falk, M.L., Langer, J.S.: Dynamics of viscoplastic deformation in amorphous solids. Phys. Rev. E **57**, 7192–7205 (1998)
16. Demkowicz, M.J., Argon, A.S.: High-density liquid-like component facilitates plastic flow in a model amorphous silicon system. Phys. Rev. Lett. **93**, 025505 (2004)
17. Argon, A.S., Demkowicz, M.J.: What can plasticity of amorphous silicon tell us about plasticity of metallic glasses. Metall. Mater. Trans. A **39**, 1762–1778 (2008)
18. Jäger, H.U., Albe, K.: Molecular-dynamics simulations of steady-state growth of ion-deposited tetrahedral amorphous carbon films. J. Appl. Phys. **88**, 1129–1135 (2000)
19. Pastewka L., Pou P., Perez R., Gumbsch P., Moseler M. (2008) Describing bond-breaking processes by reactive potentials Importance: of an environment-dependent interaction range. Phys. Rev. B 78:161402(R)
20. Liu, Y., Erdemir, A., Meletis, E.I.: A study of the wear mechanism of diamond-like carbon films. Surf. Coat. Technol. **82**, 48–56 (1996)
21. Harrison, J.A., Brenner, D.W.: Simulated tribochemistry: an atomic-scale view of the wear of diamond. J. Am. Chem. Soc. **116**, 10399–10402 (1994)
22. Pastewka, L., Moser, S., Moseler, M.: Atomistic insights into the running-in, lubrication, and failure of hydrogenated diamond-like carbon coatings. Tribol. Lett. **39**, 49–61 (2010)
23. Pastewka, L., Moser, S., Moseler, M., Blug, B., Meier, S., Hollstein, T., Gubsch, P.: The running-in of amorphous hydrocarbon tribocoatings: a comparison between experiment and molecular dynamics simulations. Int. J. Mater. Res. **10**, 1136–1143 (2008)
24. Brenner, D.W., Shenderova, O.A., Harrison, J.A., Stuart S., J., Ni, B., Sinnott, S.B.: A second-generation reactive empirical bond order (REBO) potential energy expression for hydrocarbons. J. Phys. Condens. Matter. **14**, 783–802 (2002)
25. Pastewka, L., Klemenz, A., Gumbsch, P., Moseler, M.: Screened empirical bond-order potentials for Si-C. Phys. Rev. B **87**, 205410 (2013)
26. Pastewka, L., Mrovec, M., Moseler, M., Gumbsch, P.: Bond order potentials for fracture, wear, and plasticity. MRS Bull. **37**, 493–503 (2012)
27. Field J., E.: . The Properties of Natural and Synthetic Diamond, Academic Press, London (1992)
28. Sumant A., V., Grierson, D.S., Gerbi, J.E., Carlisle, J.A., Auciello, O., Carpick, R.W.: Surface chemistry and bonding configuration of ultrananocrystalline diamond surfaces and their effects on nanotribological properties. Phys. Rev. B **76**, 235429 (2007)
29. Casiraghi, C., Ferrari, A.C., Ohr, R., Chu, D., Robertson, J.: Surface properties of ultra-thin tetrahedral amorphous carbon films for magnetic storage technology. Diam. Relat. Mater. **13**, 1416–1421 (2004)
30. Matta, C., Barros Bouchet, M.I., Le-Mogne, T., Vachet, B., Martin, J.M., Sagawa, T.: Tribochemistry of tetrahedral hydrogen-free amorphous carbon coatings in the presence of OH-containing lubricants. Lubr. Sci. **20**, 137–149 (2008)
31. Bitzek, E., Koskinen, P., Gähler, F., Moseler, M., Gumbsch, P.: Structural relaxation made simple. Phys. Rev. Lett. **97**, 170201 (2006)
32. Angadi, M.A., Watanabe, T., Bodapati, A., Xiao, X., Auciello, O., Carlisle, J.A., Eastman, J.A., Keblinski, P., Schelling, P.K., Phillpot, S.R.: Thermal transport and grain boundary conductance in ultrananocrystalline diamond thin films. J. Appl. Phys. **99**, 114301 (2006)
33. Balandin, A.A.: Thermal properties of graphene and nanostructured carbon materials. Nat. Mat. **10**, 569–581 (2011)
34. Hird, J.R., Field, J.E.: Diamond polishing. Proc. R. Soc. Lond. A **460**, 3547–3568 (2004)
35. Moras, G., Pastewka, L., Walter, M., Schnagl, J., Gumbsch, P., Moseler, M.: Progressive shortening of sp-hybridized carbon chains through oxygen-induced cleavage. J. Phys. Chem. C **115**, 24653–24661 (2011)
36. Moras, G., Pastewka, L., Gumbsch, P., Moseler, M.: Formation and oxidation of linear carbon chains and their role in the wear of carbon materials. Tribol. Lett. **44**, 355–365 (2011)
37. Krishnan, M., Nalaskowski, J.W., Cook, L.M.: Chemical mechanical planarization: slurry chemistry, materials, and mechanisms. Chem. Rev. **110**, 178–204 (2010)
38. Moseler, M., Gumbsch, P., Casiraghi, C., Ferrari, A.C., Robertson, J.: The ultrasmoothness of diamond-lime carbon. Science **309**, 1545 (2005)
39. Davis, C.A., Amaratunga, G.A.J., Knowles, K.M.: Growth mechanism and cross-sectional structure of tetrahedral amorphous carbon thin films. Phys. Rev. Lett. **80**, 3280 (1998)
40. Merkle, A., Marks, L.P.: Liquid-like tribology of gold studied by in situ TEM. Wear **265**, 1864–1869 (2008)
41. Mndange-Pfupfu, A., Eryilmaz, O., Erdemir, A.: Quantification of sliding-induced phase transformation in N3FC diamond-like carbon films and L.D. Marks. Diam. Relat. Mater. **20**, 1143–1148 (2011)
42. Mndange-Pfupfu, A., Ciston, J., Eryilmaz, O., Erdemir, A., Marks, L.D.: Direct observation of tribochemically assisted wear on diamond-like carbon thin films. Tribol. Lett. **49**, 351–356 (2013)